Supplement of Clim. Past, 21, 2283–2297, 2025 https://doi.org/10.5194/cp-21-2283-2025-supplement © Author(s) 2025. CC BY 4.0 License.





Supplement of

Increasing opal productivity in the Late Eocene Southern Ocean: Evidence for increased carbon export preceding the Eocene-Oligocene glaciation

Volkan Özen et al.

Correspondence to: Volkan Özen (volkan.oezen@fu-berlin.de)

The copyright of individual parts of the supplement might differ from the article licence.

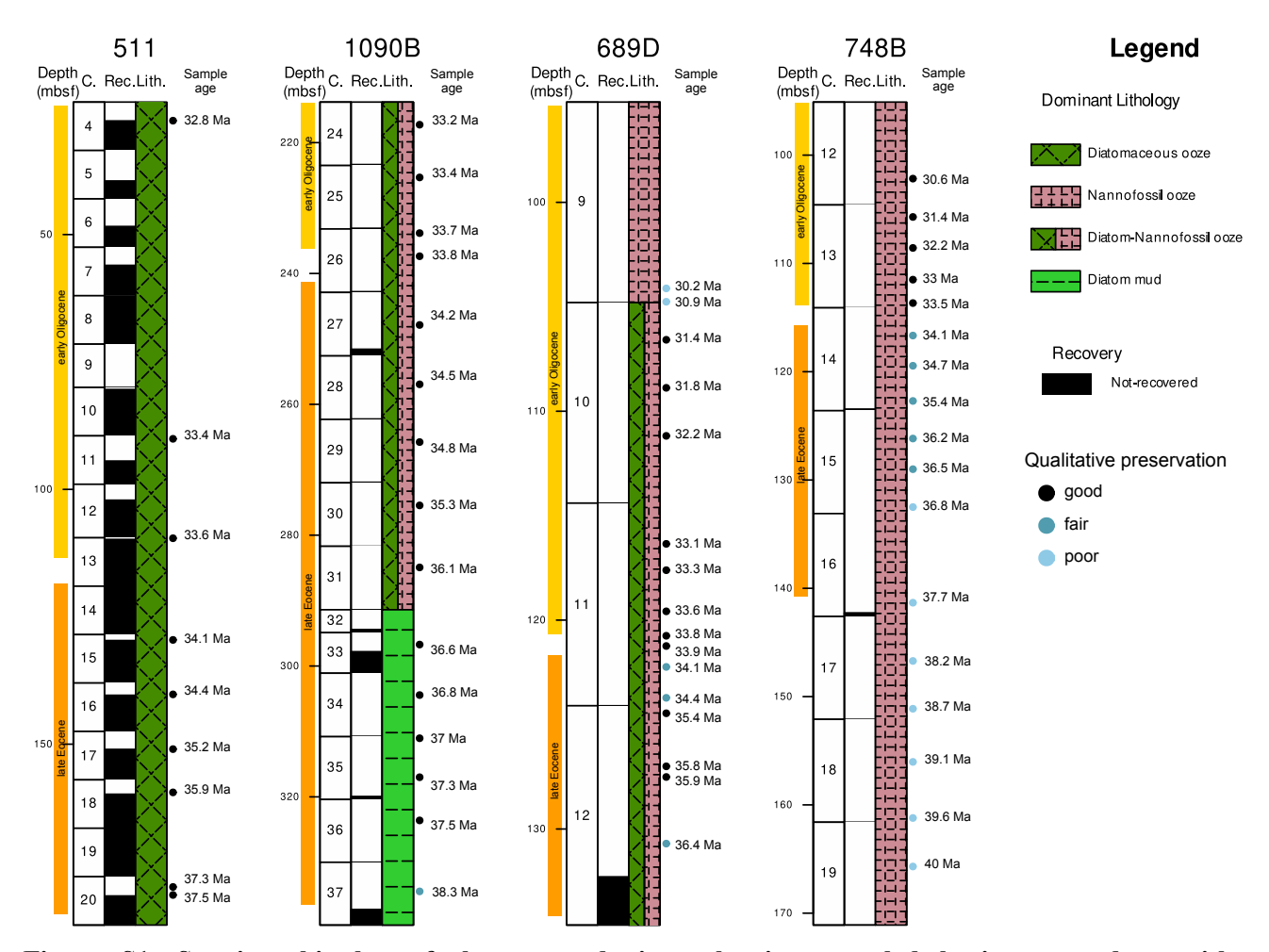


Figure S1. Stratigraphic log of the targeted sites, showing sampled horizons as dots, with corresponding age (Ma), positioned alongside the stratigraphic columns. Dots are color-coded to indicate the assessed qualitative preservation of the corresponding samples (see figure legend). Examples of each preservation category can be found in Figures S9-11. Corresponding samples for each datum can be found in Southern Ocean Diatom MAR data.

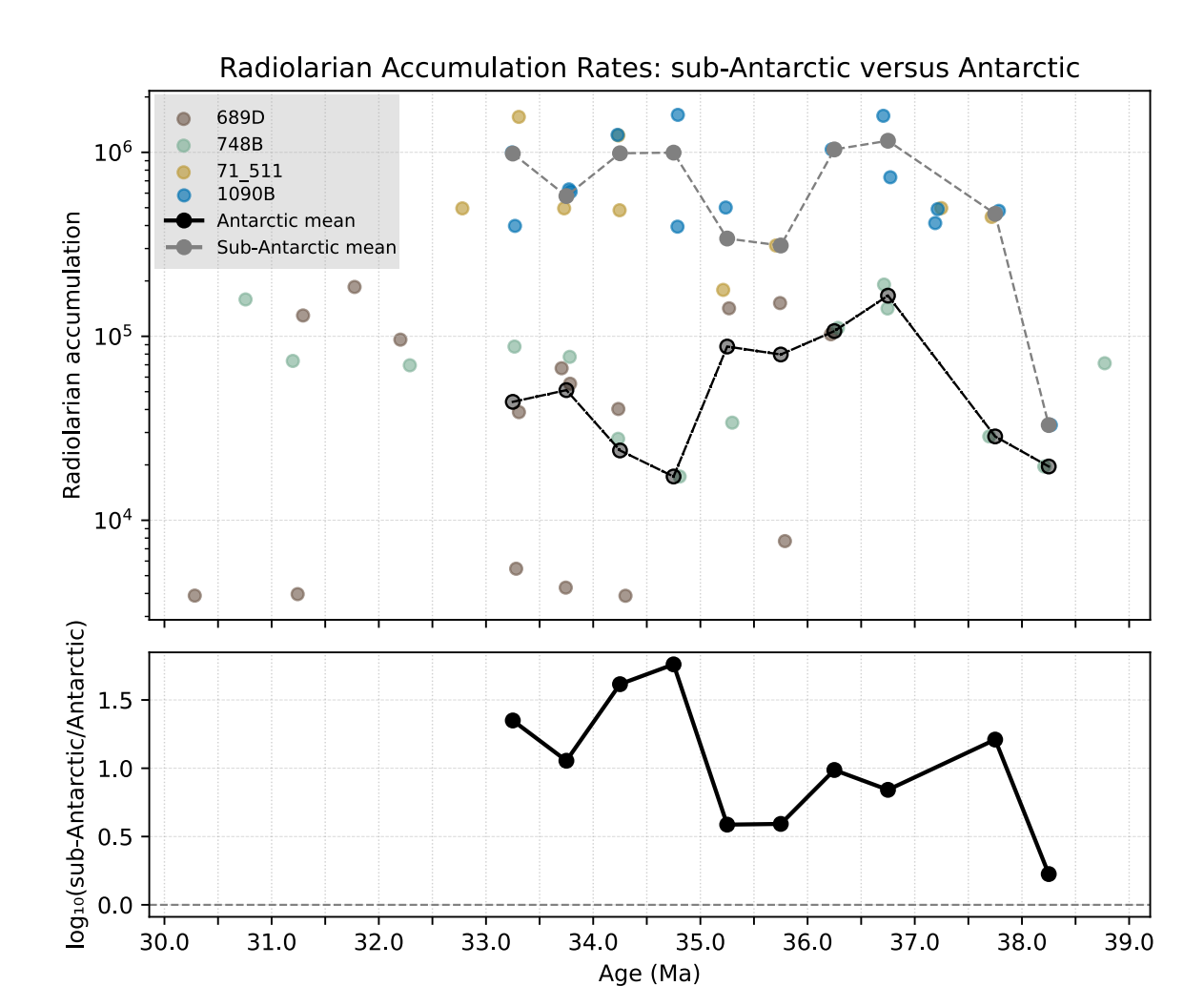


Figure S2. Upper: Radiolarian accumulation rates (radiolarian cm⁻² kyr⁻¹) form sub-Antarctic sites (DSDP 511 and ODP 1090) compared with Antarctic sites (ODP 689 and 748). Data are grouped into 0.5 Ma bins, and mean values were calculated from all samples within each bin for each region. The black (dashed) line shows the mean trend for Antarctic sites, and gray (dashed) line represent the sub-Antarctic sites. Lower: Difference between Antarctic and sub-Antarctic means, revealing a state shift and widening gap after ~35.5 Ma.

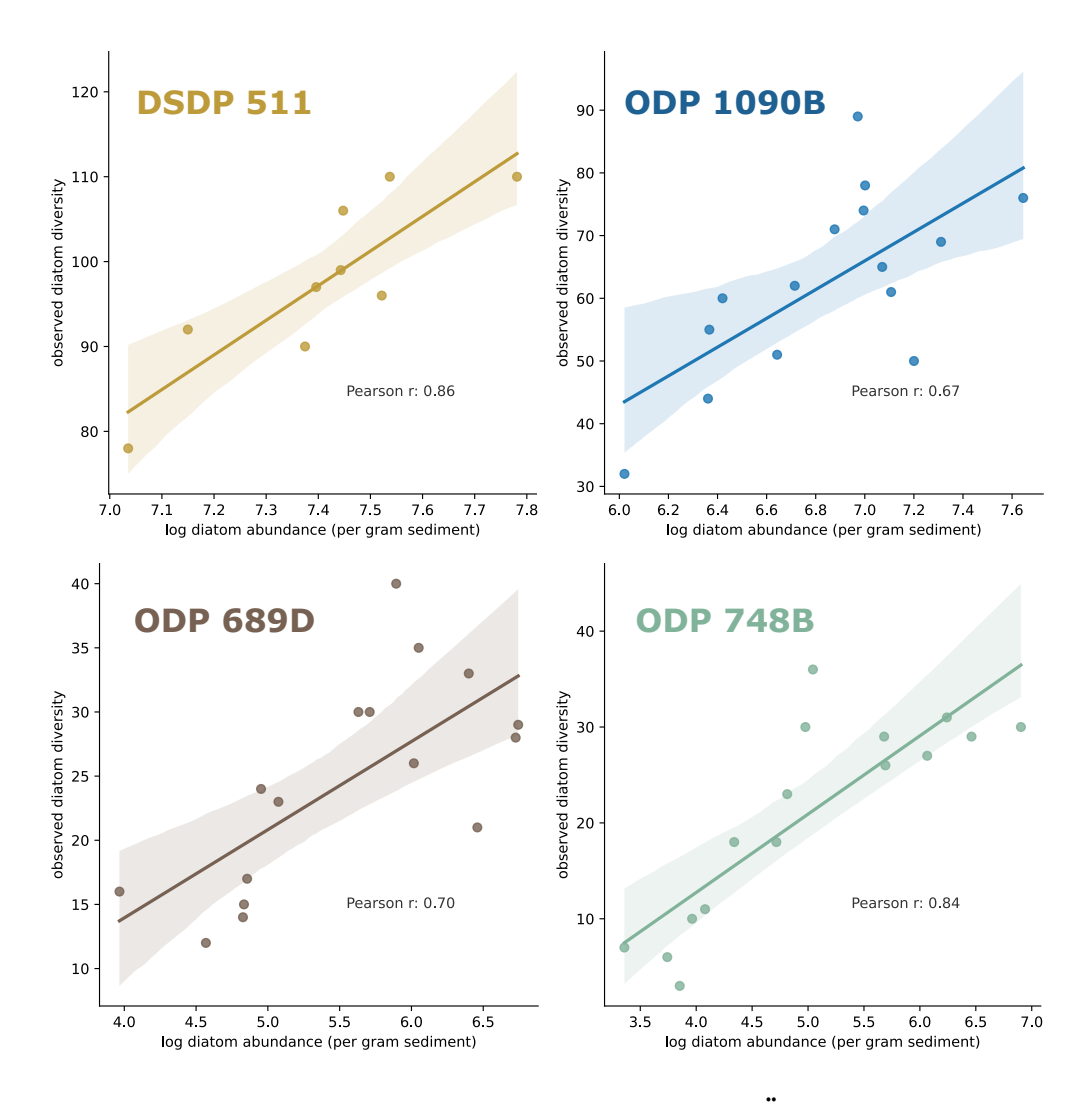


Figure S3. Site-specific correlations between diatom diversity (Özen et al., subm.) and diatom abundance (log scale) per gram of sediment. Accumulation rates were not used to minimize the effect of age-model uncertainties. For each site, trend lines are shown with 95% confidence intervals, together with the Pearson correlation coefficient between diversity and abundance. Pearson correlations and confidence intervals were calculated using Python's SciPy module (v1.15.3).

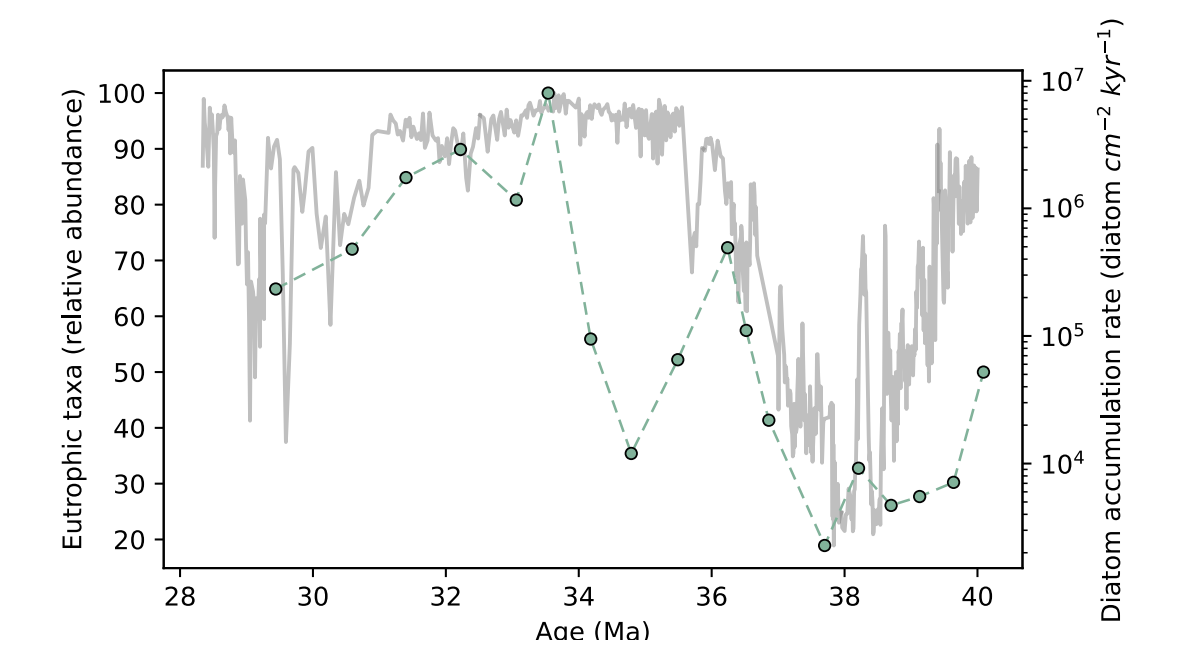


Figure S4. Kerguelen Plateau productivity dynamics across the EOT. Comparison of eutrophic nannofossil relative abundances from Villa et al. (2014) with diatom MAR (this study).

113_689B BFAR after Diester-Haas and Zahn 1996

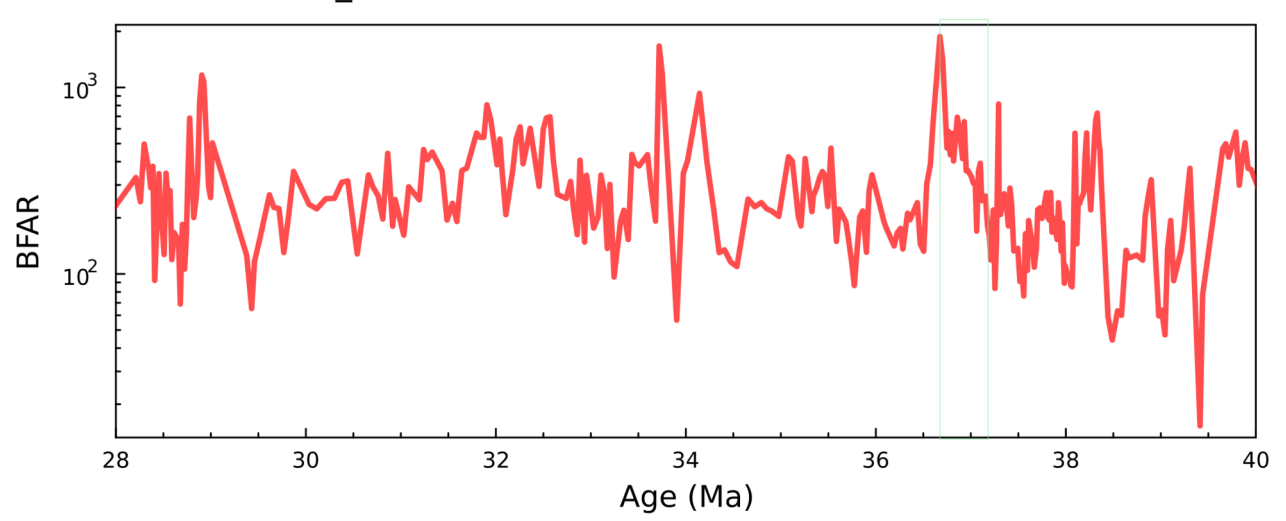


Figure S5. Benthic foraminifera accumulation rates (benthic foraminifera cm⁻² kyr⁻¹) from Diester-Haass and Zahn (1996), updated using our revised age model for ODP Site 689.

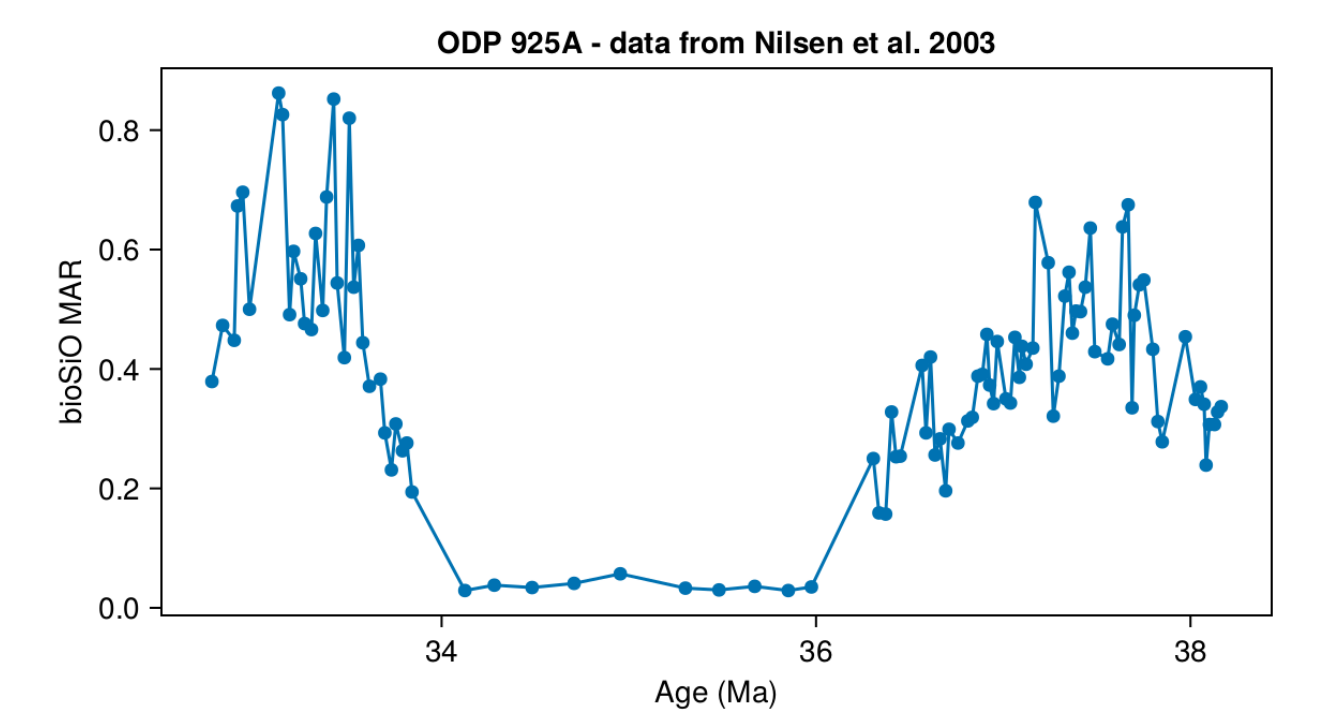


Figure S6. Opal record from the equatorial Atlantic. Opal accumulation data from Nilsen et al. (2013) illustrate a characteristic two-pulse pattern observed across multiple sites, with varying degrees and magnitudes. The first pulse occurs around ~38–36 Ma, followed by a second pulse in the earliest Oligocene.

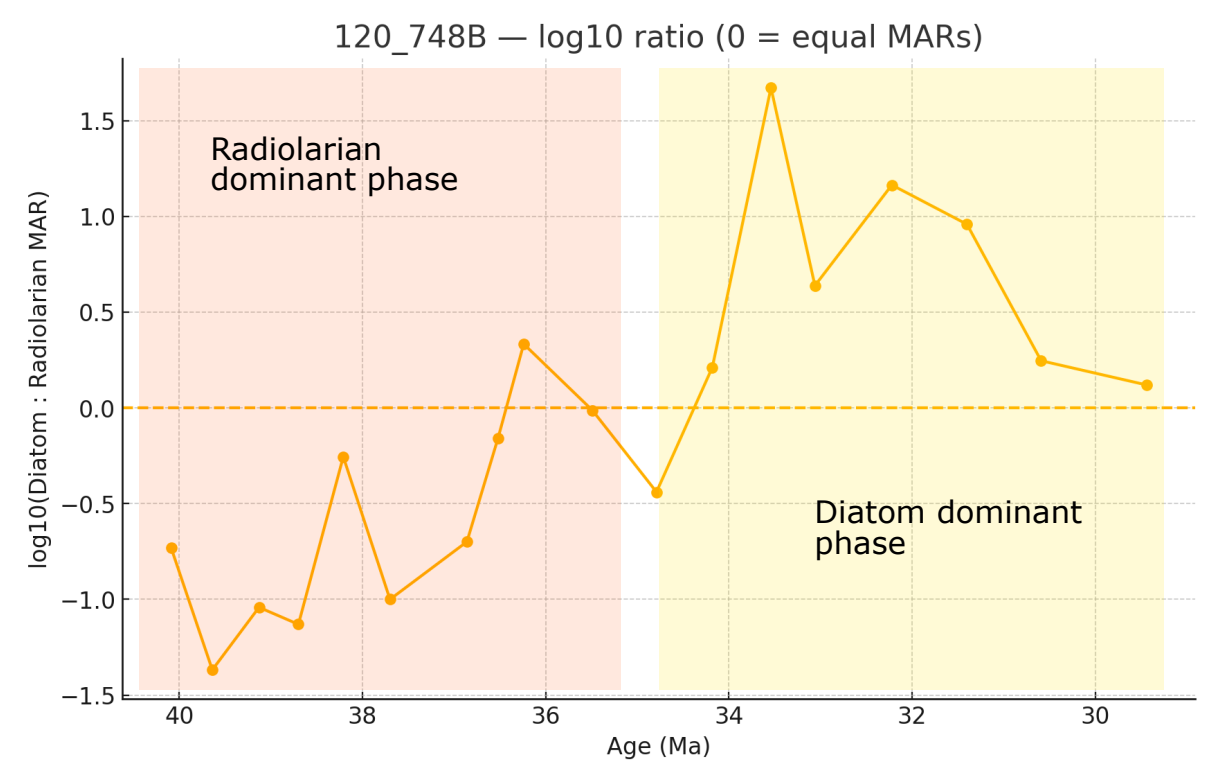


Figure S7. Difference between diatom and radiolarian mass accumulation rates (MARs) across the EOT at ODP Site 748. Negative values indicate intervals where radiolarians are more abundant, and positive values indicate intervals where diatoms dominate.

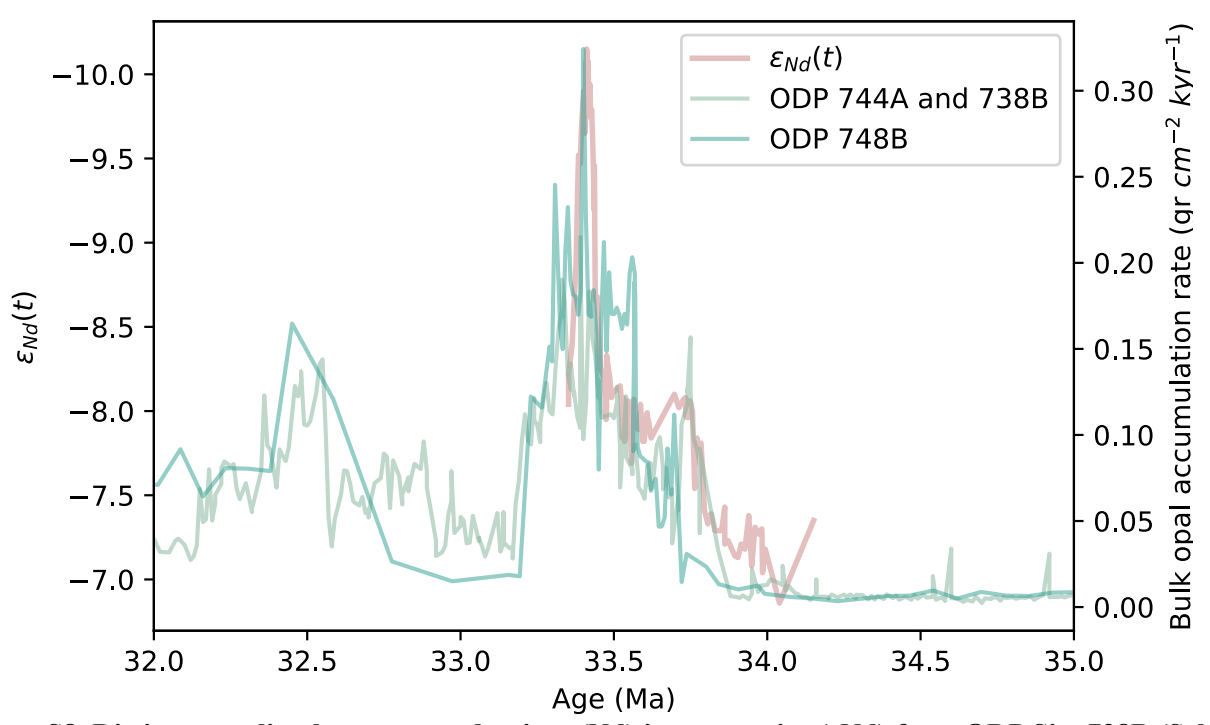
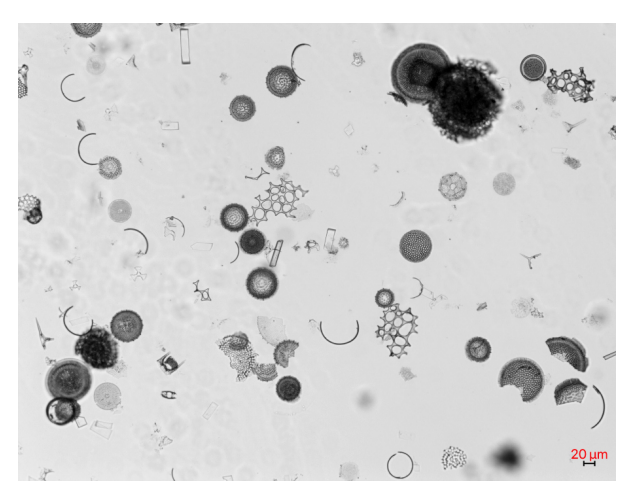


Figure S8. Distinct coupling between neodymium (Nd) isotope ratios (εNd) from ODP Site 738B (Scher et al., 2011) and bulk opal accumulation rates from the same region (ODP Sites 744A and 748B; Salamy and Zachos, 1999; Brylka et al., 2024). Data points for both proxies have been updated using our revised age models.



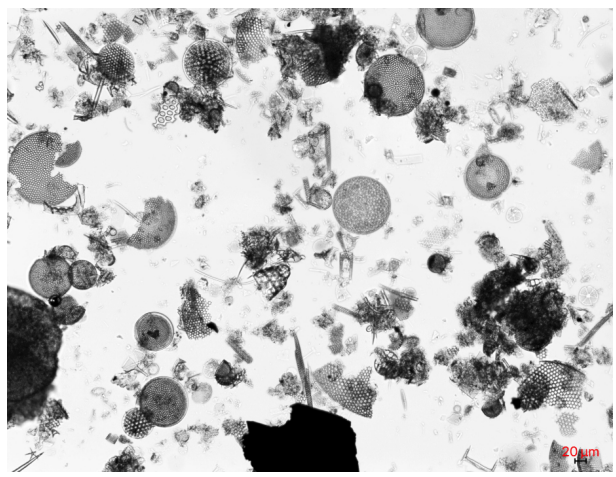
748B-13-03,97 (108.57 mbsf). **Preservation: good**. Diatom density is significantly lower than at ODP 1090 and DSDP 511; nevertheless, specimens with fine structures are present.



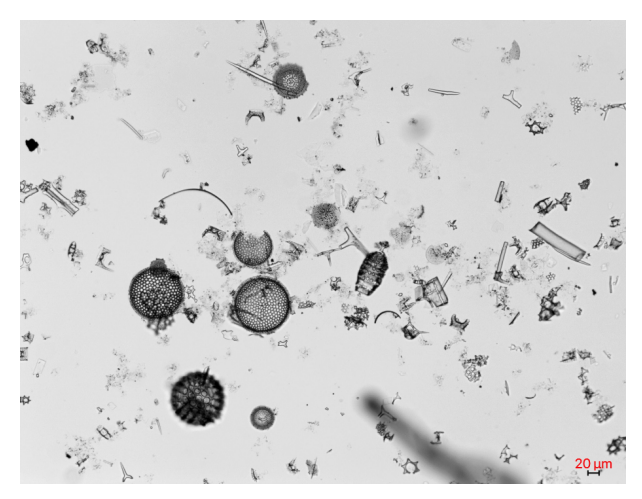
748B-13-07,6 (113.66 mbsf). **Preservation: good**. Likewise, density is relatively low, yet most specimens are complete and can be readily identified to the species level.



1090B-30-03,45 (275.45 mbsf). **Preservation: good**.

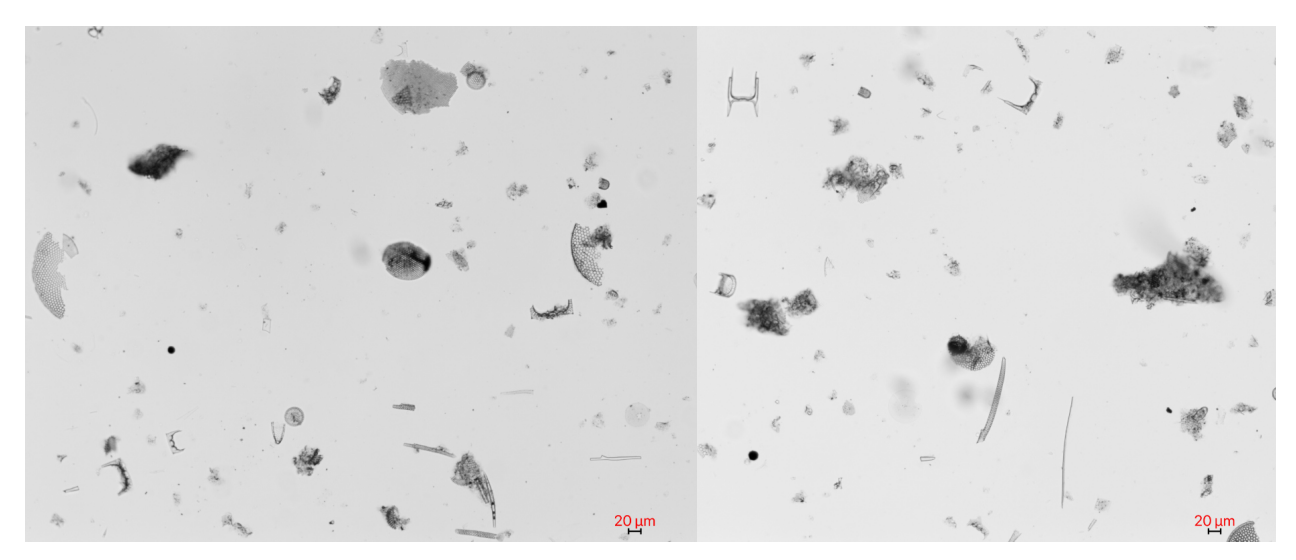


511-18-02,96 (159.46 mbsf). **Preservation: good**.

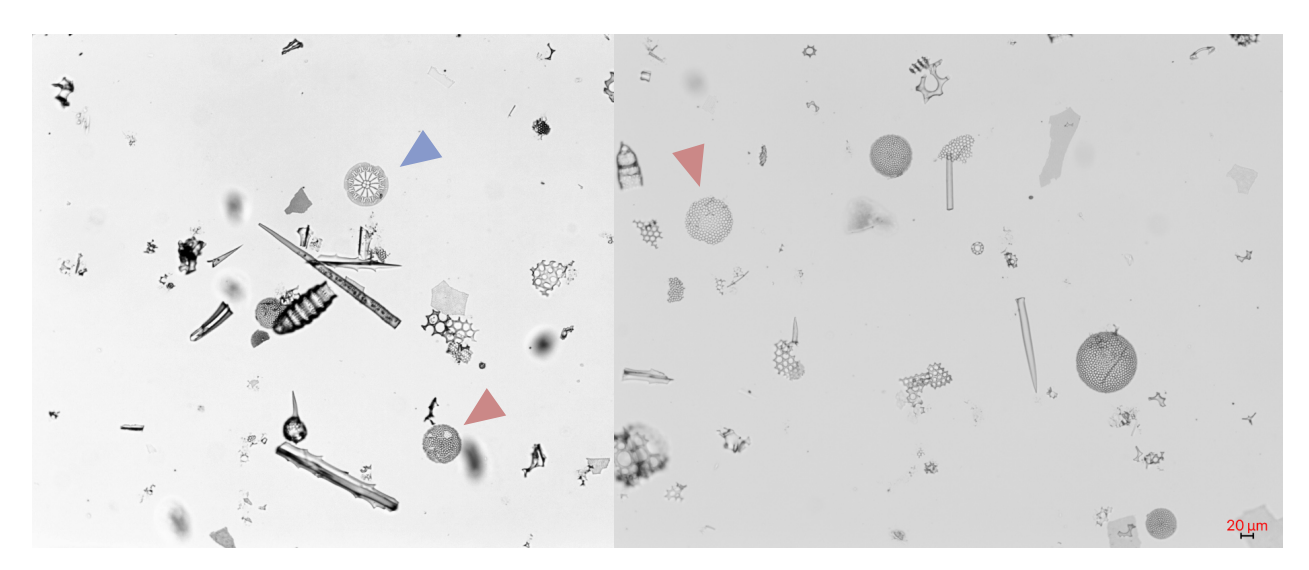


689D-10-03,106 (108.88mbsf). **Preservation: good**. Specimen density is low, giving the imression of poor preservation; yet specimens are as intact and morphological characters are easily tracable as in, for example, 748B-13-03,97.

Figure S9. Example of samples assessed as having 'good' preservation. Each panel includes the sample name and depth with accompanying notes.

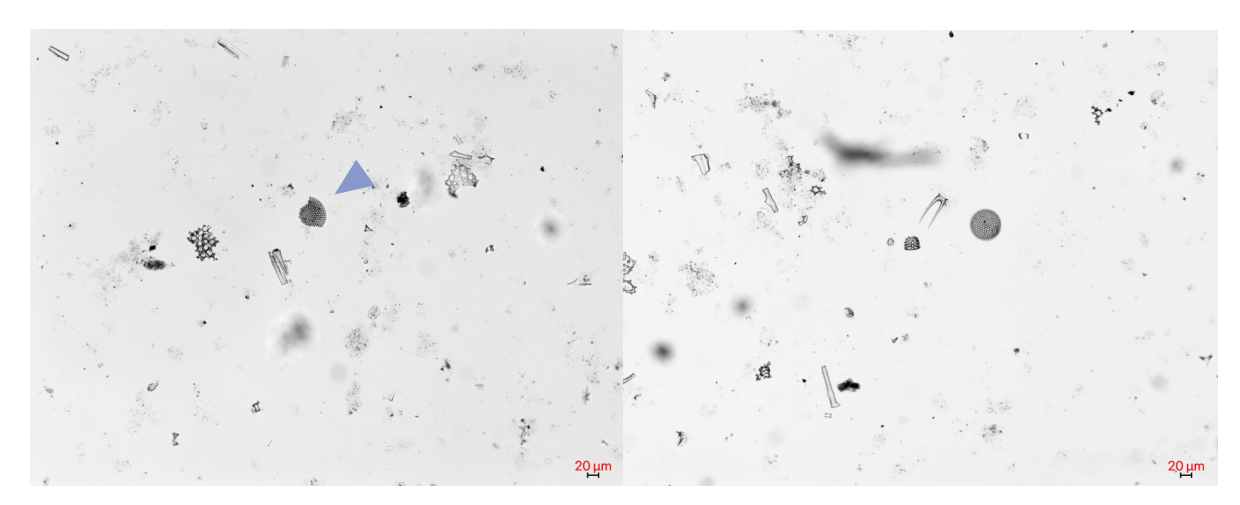


511-12-01,57 (99.57 mbsf). **Preservation: fair**. Due to the high level of fragmentation, such samples are classified as having fair preservation.

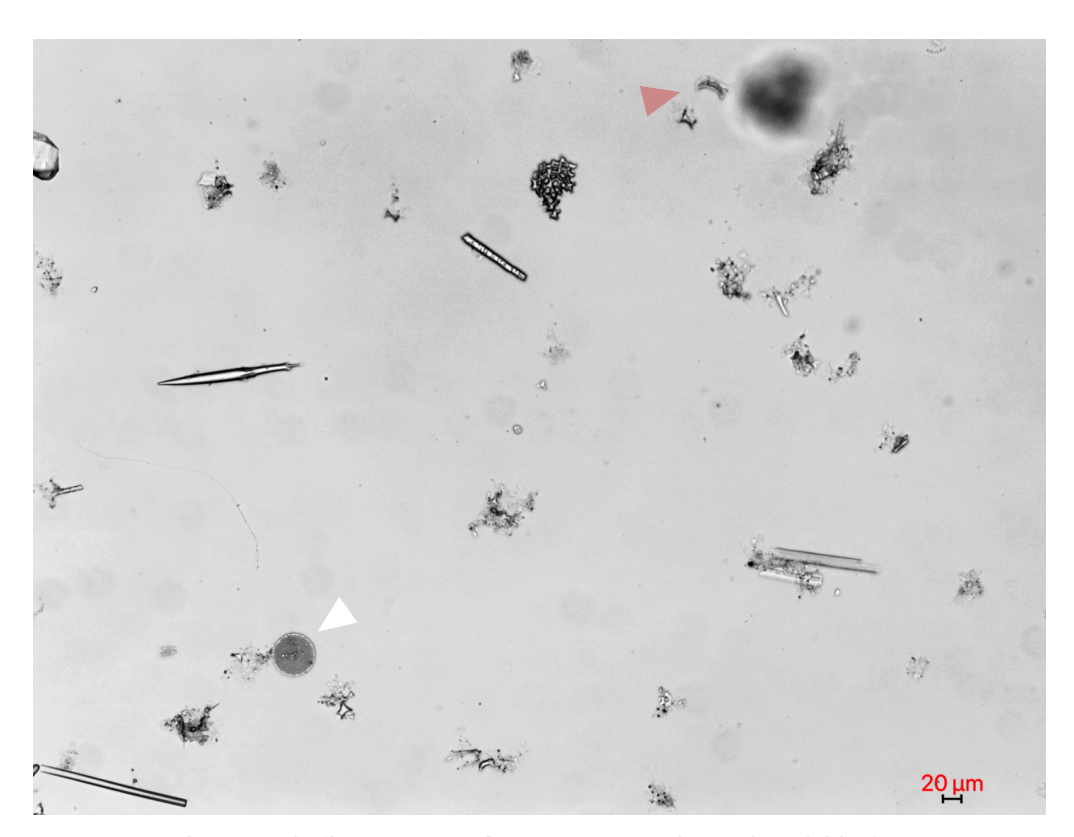


748B-15-02,107 (126.17 mbsf). **Preservation: fair**. Dissolution relicts (red trianlgle) are present, yet still specimens of dissolution-susceptible species (e.g., *Asterolampra vulgaris*, see blue triangle) still exhibit a high degree of completeness and fine morphological details.

Figure S10. Example of samples assessed as having 'fair' preservation. Each panel includes the sample name and depth with accompanying notes.



689D-09-06,142 (104.12 mbsf). **Preservation: poor**. The most dissolution resistent groups (e.g., genus *Stephanopyxis*) show high degree fragmentation (left). Species remain tracable (right, *Hemiaulus incisus* and *Coscinodiscus marginatus*), yet exhibit sign of dissolution relicts in the valve periphery.



748B-15-06,140 (132.5 mbsf). **Preservation: poor**. Mostly unidentifable fragments are present (red triangle, *Hemiaulus* fragment). However, occasional specimens with dissolution relicts along the valve preiphery retain identifiable morphological features (white arrow, *Azpeitia oligocenicus*).

Figure S11. Example of samples assessed as having 'poor' preservation. Each panel includes the sample name and depth with accompanying notes.